Robust Cooperative Load Frequency Control for Enhancing Wind Energy Integration in Multi-Area Power Systems

Zhijian Hu, Kun Zhang, Rong Su, Ruiping Wang

Robust Cooperative Load Frequency Control for Enhancing Wind Energy Integration in Multi-area Power Systems

Zhijian Hu, *Member, IEEE*, Kun Zhang, *Member, IEEE*, Rong Su, *Senior Member, IEEE*, and Ruiping Wang

***Abstract*—The wind energy, as a kind of renewable energy resources, has the potential to replace traditional fossil fuels. However, its intermittent power output can incur frequency instability due to the instantaneous unbalance between power generation and load demand. To smooth the penetration of wind energy, this paper presents a robust cooperative load frequency control (LFC) strategy for multi-area power systems, which is a hierarchical control approach. For the low-level wind turbine control, this paper adopts model predictive control (MPC) method to achieve the rated wind power tracking. In the meantime, an improved event-triggered scheme (ETS) considering multiple historic released signals is employed to relieve the computational burden of MPC. For the high-level cooperative LFC, this paper incorporates the robust performance index in the control synthesis to suppress the impact of intermittent wind power on frequency stability. In addition, to address the underlying shift of the steady-state operating point caused by the intermittent wind power supply, this paper improves the commonly used small-signal LFC model by adding an uncertain matrix, which reasonably explains the possible change of system parameters and extends the applicability of the traditional LFC model. Simulations are done on a four-area power system, and the results verify the efficacy of the presented event-triggered scheme and the robust cooperative LFC approach.**

***Note to Practitioners*—To promote the penetration of wind energy into power systems, this work explores a robust cooperative LFC approach under multi-agent structure to ensure the stability of the system, aiming at extending the applicability of existing approaches. The proposed approach is hierarchical. At the rated wind power tracking level, the MPC is employed to handle constraints associated with actuating devices, such as heterogeneous convertors. Simultaneously, an improved ETS considering multiple historic triggered signals is integrated in the MPC to reduce the computational burden. At the power system level, the robust performance index is incorporated in the control design to smooth the impacts of intermittent wind power on frequency stability. Additionally, the study accounts for the potential shift of the steady-state operating point and improves the traditional small-signal LFC model by adding an uncertain matrix, which can better explain the variation of system parameters and is more applicable in practical power system engineering. Simulation results demonstrate that the proposed robust cooperative LFC approach can effectively maintain the system frequency within the admissible range under the high penetration of wind energy, whereas the traditional PI controller falls short in this regard.**

***Index Terms*—Load frequency control, wind turbines, multi-area power systems, model predictive control, event-triggered scheme.**

This work is supported in part by the European Union's Horizon 2022 Research and Innovation Programme for the Marie Skłodowska-Curie Actions (101108472), in part by the National Natural Science Foundation of China (62103408), in part by A*STAR under its RIE2020 Advanced Manufacturing and Engineering (AME) Industry Alignment Fund-Pre Positioning (IAF-PP) (Award A19d6a0053), in part by A*STAR under its IAF-ICP Programme I2001E0067 and the Schaeffler Hub for Advanced Research at NTU, and in part by European Horizon 2020 Marie Skłodowska-Curie Actions (101023244). (*Corresponding author: Kun Zhang.*)

Zhijian Hu is with LAAS-CNRS, Université de Toulouse, CNRS, Toulouse 31400, France and also with the School of Electrical and Electronic Engineering, Nanyang Technological University, 639798, Singapore. (e-mail: huzhijian1991@gmail.com).

Rong Su is with the School of Electrical and Electronic Engineering, Nanyang Technological University, 639798, Singapore (e-mail: rsu@ntu.edu.sg).

Kun Zhang is with the School of Astronautics, Beihang University, Beijing 100191, China (e-mail: nukgnahz@163.com).

Ruiping Wang is with the School of Computer Science and Engineering, Nanyang Technological University, 639798, Singapore (Emails: ruiping.wang@ntu.edu.sg).

Yushuai Li is with the Department of Informatics, University of Oslo, Oslo 0316, Norway (e-mail: yushuaili@ieee.org).

I. INTRODUCTION

In recent decades, the cooperative control technology in multi-agent systems has drawn wide attention in the context of achieving a common goal through collaborative efforts and shared information [1]–[5]. As a typical application of multi-agent systems [6], [7], the cooperative LFC for multi-area power systems demonstrates superior performance in fastly and accurately recovering the frequency when one or more areas suffer load disturbances, compared to its non-cooperative control counterparts. As a consequence, the work is to investigate a cooperative LFC approach for interconnected power systems with partial state information sharing, such as load frequency and tie-line power signals.

Distributed renewable energy sources (DRESs) are promising supplements of traditional fossil fuels, considering the sustainable development of both economy and environment [8]–[11]. Among them, the wind power accounts for the largest proportion due to the easy deployment on either offshore or onshore regions. To take full advantage of wind energy, two perspective control modes of wind turbines have been investigated based on the wind speed, namely maximal power point tracking (MPPT) and rated power tracking [12]. In situations where the wind speed surpasses the cut-in threshold yet remains below the rated speed, the MPPT control technique is utilized to optimize the energy output in line with the wind profile. Conversely, when the wind speed exceeds the rated limit but remains below the cut-off threshold, the rated power tracking control mechanism is employed to ensure that the output power remains constant. As for the control design, a flood of theoretical investigations has been carried out, e.g., robust control [13], [14], model predictive control (MPC)

[15]–[19], and learning-based control [20]–[23]. The MPC method performs superior application prospects in wind power generations due to the unique advantages in jointly addressing finite-horizon optimization and control, and in integrating state constraints. The authors in [16] presented a coordinated MPC strategy for wind energy dominated power system by simultaneously considering the generation rate constraints, load disturbance changes, and the wind speed constraints. The authors in [18] investigated the structural loadings of wind turbines, which enhances the active power tracking performance under MPC. However, the above results ignored the computational burden during the implementation of MPC, which is a prerequisite to ensure that the optimal control action can be selected out within the adjacent sampling instants.

While wind energy contributes significantly to the sustainability of electrical power, its growing integration may introduce instability to the main grid. This instability arises from the absence of the physical inertia that synchronous generators offer in conventional power systems [24]–[27]. Moreover, different from the load disturbances, the intermittent nature of wind power supply introduces a distinct challenge by inducing substantial load imbalances, thereby necessitating a shift in the system's operating point. In such instances, the traditional small-signal model [24], [28]–[32], typically linearized at a singular steady-state operating point, loses accuracy due to the shift of the steady-state operating point. To account for this category of inaccuracies stemming from the outlined modeling concerns, the work of [33] systematically accommodated variations in the speed droop coefficient when formulating the governor dynamics model. Nevertheless, the approach advanced in [33] exhibits constrained applicability, as it exclusively addresses alterations in the speed droop coefficient, thereby presenting limitations in capturing the broader spectrum of system parameter variations accompanying with the shift of the steady-state operating point. However, a notable paucity of emphasis on the precise modeling of LFC exists, especially concerning the potential shift of the steady-state operating point.

Encouraged by aforementioned reviewed studies, we propose a robust cooperative LFC approach for multi-area power systems to smooth the high penetration level of wind energy with the frequency stability guarantees. Compared to the existing ones, the main differences of our work are highlighted in Table I.

The primary contributions lie in the following three aspects.

- To promote wind energy penetration and suppress the fluctuations of intermittent wind power output on system stability, a hierarchical control structure of strong universality is proposed, which is capable to provide some references to power designers and managers. At the low-level wind turbine control, the MPC method is employed to track the rated wind power, while at the high-level LFC, the robust performance index is incorporated control law derivation. Two theorems are derived to facilitate the selection of robust cooperative controller gains.

- To alleviate the computational burden of MPC implementation for rated wind power tracking, an improved event-triggered scheme (ETS) is proposed. Compared to the existing ETSs in [33]–[36], the improved ETS considers multiple historic released signals, which yields two noteworthy benefits. Firstly, it ensures the activation of specific critical points situated at the crest or trough of the state response curves. Secondly, it averts the triggering of insignificant points that may arise due to the abrupt load disturbances

- To address the potential shift of the steady-state operating point caused by intermittent wind power, this paper augments the traditional small-signal LFC model with an uncertain but bounded matrix. It is an extension of [33] that merely considered the potential change of the speed droop coefficient in modeling the governor dynamic. The improved LFC model can reasonably explain the variation of all system parameters, thus enhancing the accuracy and applicability of the LFC model.

Fig. 1 shows the framework of this work. As for the meanings of each symbol, we will give a detailed explanation in the subsequent sections that are arranged as below. Section II designs the MPC for rated wind power tracking and the improved ETS. Section III presents the robust cooperative LFC with wind turbines integration. Section IV tests the efficacy of the presented robust cooperative LFC method. Section V

TABLE I
DIFFERENCES OF OUR WORK WITH THE EXISTING STUDIES

Methods / Attributes	[1]	[6]	[7]	[10]	[11]	[15]	[16]	[24]	[28]	[29]	[30]	[31]	[32]	[33]	**Proposed**
Wind turbine	✓	✓	×	✓	✓	×	✓	×	✓	×	✓	×	×	×	✓
ETS	×	✓	×	×	×	×	×	×	×	×	×	✓	×	✓	✓
Memory-based ETS	×	×	×	×	×	×	×	×	×	×	×	×	×	×	✓
Parameter uncertainty	✓	×	×	✓	✓	×	×	×	✓	×	×	×	✓	✓	✓
Distributed control	×	✓	✓	×	×	✓	✓	✓	✓	×	×	✓	✓	✓	✓
$\mathscr{H}_\infty$ robustness	×	×	×	×	×	×	×	✓	×	✓	×	✓	✓	×	✓
Steady-state shift	×	×	×	×	×	×	×	×	×	×	×	×	×	×	✓

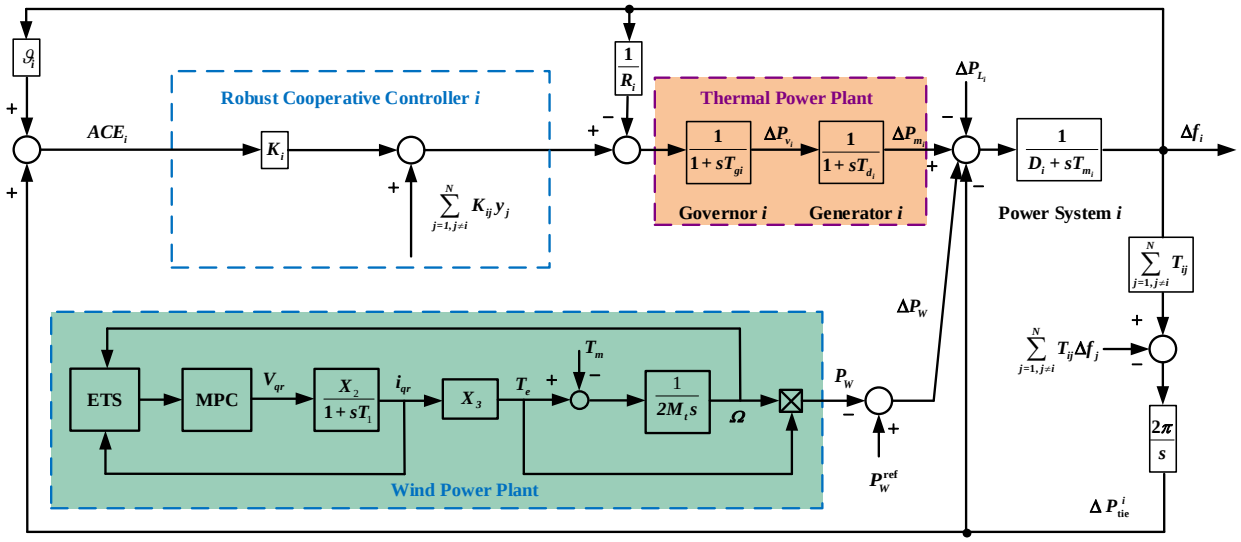

Fig. 1. Framework of the robust cooperative LFC for multi-area power systems with wind turbines.

concludes the work.

II. MPC FOR RATED WIND POWER TRACKING AND IMPROVED ETS

A. Modeling of Wind Turbines

This work avoids discussing the modeling issues of a complete wind power generation system, usually consisting of aerodynamics, drive train, generator, etc., while employs a simplified double fed induction generator (DFIG) to simulate the actual wind power supply [37]. The system dynamics of the DFIG can be described as

$$\dot{i}_{qr} = -\left(\frac{1}{T_1}\right) i_{qr} + \left(\frac{X_2}{T_1}\right) V_{qr}, \tag{1}$$

$$\dot{\Omega} = -\left(\frac{X_3}{2M_t}\right) i_{qr} + \left(\frac{1}{2M_t}\right) T_m, \tag{2}$$

where $X_2 = 1/R_r$, $T_1 = L_0/(\Omega_s R_s)$, $X_3 = L_m/L_{ss}$, $T_e = X_3 i_{qr}$, $L_0 = L_{rr} + L_m^2/L_{ss}$, $P_W = \Omega T_e$, $L_{ss} = L_s + L_m$, and $L_{rr} = L_r + L_m$; Ω is the rotational speed; T_e and T_m are the electromagnetic and mechanical torques, respectively; i_{qr} and V_{qr} are the q axial component of the rotor current and voltage, respectively; M_t is the equivalent inertia constant; L_m is the magnetization inductance; $R_r(R_s)$ is the rotor (stator) resistance; $L_r(L_s)$ is the rotor (stator) leakage inductance; $L_{rr}(L_{ss})$ is the rotor (stator) self induction; Ω_s is the synchronous rotational speed.

The state-space representation of (1)-(2) is

$$\begin{cases} \dot{x}_W = \mathscr{A}_{\mathscr{W}} x_W + \mathscr{B}_{\mathscr{W}} u_W + \mathscr{F}_{\mathscr{W}} v_W, \\ y_W = \mathscr{C}_{\mathscr{W}} x_W, \end{cases} \tag{3}$$

where $x_W = [i_{qr} \quad \Omega]^T$ is the state vector; $u_W = V_{qr}$ is the control input; $v_W = T_m$ is the electromagnetic disturbance; y_W is the output vector with $\mathscr{C}_W = \text{diag}\{1, 1\}$;

$$\mathscr{A}_{\mathscr{W}} = \begin{bmatrix} \frac{-1}{T_1} & 0 \\ \frac{-X_3}{2M_t} & 0 \end{bmatrix}, \mathscr{B}_{\mathscr{W}} = \begin{bmatrix} \frac{X_2}{T_1} \\ 0 \end{bmatrix}, \mathscr{F}_{\mathscr{W}} = \begin{bmatrix} 0 \\ \frac{1}{2M_t} \end{bmatrix}.$$

Since all state signals used in rated wind power tracking control are measured by digital devices, equation (3) is discretized as

$$\begin{cases} x_W(k+1) = A_W x_W(k) + B_W u_W(k) + F_W v_W(k), \\ y_W(k) = C_W x_W(k), \end{cases} \tag{4}$$

where $A_W = e^{\mathscr{A}_{\mathscr{W}} h}$; $B_W = \int_0^h e^{\mathscr{A}_{\mathscr{W}} h} \mathscr{B}_{\mathscr{W}} dh$; $C_W = \mathscr{C}_{\mathscr{W}}$; $F_W = \int_0^h e^{\mathscr{A}_{\mathscr{W}} h} \mathscr{F}_{\mathscr{W}} dh$; h represents the sampling time.

B. MPC for Rated Wind Power Tracking

The MPC technique has drawn broad attention in the electric power sector due to its capability of combing optimization and control. MPC has emerged as a popular control approach for tracking rated wind power, particularly for addressing finite-horizon constrained problems. Three basic elements of MPC are prediction model, feedback correction, and rolling optimization. Within each iteration, the controller employs sensor measurements to calculate an optimal control sequence, executing the first element of the sequence upon the system. Subsequently, new measurements are utilized for rectifying the prediction error, thereby initiating the repetition of the optimization procedure. We design the cost function of MPC for (4) as

$$\begin{aligned} \mathcal{J}(\boldsymbol{x_W}(k), \boldsymbol{u_W}(k)) = \sum_{m=0}^{N-1} (\|x_W(k+m|k) - x_W^{\text{ref}}\|_Q^2 \\ + \|u_W(k+m|k) - u_W^{\text{ref}}\|_S^2) + V_f(x_W(k+N|k)), \end{aligned} \tag{5}$$

where $\boldsymbol{u_W}(k) = [u_W(k|k)^T \cdots u_W(k+N-1|k)^T]^T$, and $\boldsymbol{x_W}(k) = [x_W(k+1|k)^T \cdots x_W(k+N|k)^T]^T$; N signifies the

control horizon and the prediction horizon; x_W^{ref} indicates the reference state vector consisting of rated current and rotational speed; u_W^{ref} denotes the reference control vector; Q and S are two adjustable matrices; $V_f(x_W(k+N|k))$ means the terminal penalty cost, which is set as zero in this work.

Remark 1: The selection criteria for the control horizon and the prediction horizon in MPC are contingent upon the specific application and desired system performance. When employing MPC for rated wind power tracking, the target system performance typically pertains to the wind power output dynamics. The selection of control horizon should reflect the time scales at which the system responds to control inputs and disturbances. A longer control horizon may be needed for slower systems, while a shorter control horizon may suffice for faster systems. As for the selection of prediction horizon, a more extended range usually yields superior predictive results, as it encompasses a broader spectrum of anticipated system behaviors. However, this advantage is offset by a rise in computational demands. In real-world wind power generation system, the control horizon should strike a balance between accurate prediction and computational efficiency. Notably, it should never exceed the prediction horizon.

Considering the limitations of actuating devices (e.g., stator/rotor side convertors), constraints are incorporated in the control design. Then, the formal MPC for (4) is given by

$$\min_{\boldsymbol{u_W}} \mathcal{J}(\boldsymbol{x_W}(k), \boldsymbol{u_W}(k))$$

$$\text{s.t.} \begin{cases} x_W(k+m+1|k) = A_W x_W(k+m|k) \\ \qquad\qquad\qquad +B_W u_W(k+m|k), \\ x_W(k|k) = x_W(k), \\ x_W(k+N|k) \in \Theta, \\ i_{qr,\min} \le i_{qr}(k+m|k) \le i_{qr,\max}, \\ \Omega_{\min} \le \Omega(k+m|k) \le \Omega_{\max}, \\ m = 1, 2, \cdots, N, \end{cases} \tag{6}$$

where Θ confines the terminal region; $i_{qr,\min}(i_{qr,\max})$ and $\Omega_{\min}(\Omega_{\max})$ denote the current and rotational speed limitations.

C. Improved ETS

The computational burden associated with the adoption of the MPC method in rated wind power tracking has received limited attention in existing research, despite its fundamental importance, especially when longer prediction horizons are employed for those wind turbines without advanced processing units. To address this issue, our work incorporates an improved ETS into the MPC implementation, that is (7), with the objective of reducing the computational workload involved in determining the optimal control action. The improved event-triggered condition is

$$\Upsilon(k) = \sum_{p=1}^{\bar{p}} \rho^p e^p(k)^T \Phi e^p(k) - \sigma \hat{y}(k)^T \Phi \hat{y}(k) \ge 0, \tag{7}$$

where $e^p(k) = y(k) - y(k-\varepsilon^p)$, $\hat{y}(k) = \frac{1}{\bar{p}} \sum_{p=1}^{\bar{p}} y(k-\varepsilon^p)$, and $0 < \varepsilon^1 < \varepsilon^2 < \cdots < \varepsilon^{\bar{p}}$; $y(k-\varepsilon^p)$ indicates the historic triggered signal; ρ^p denotes the weighting factor of historic triggered signals satisfying $\sum_{p=1}^{\bar{p}} \rho^p = 1$; Φ signifies a diagonal matrix to capture the importancy of states; σ means a tuning factor.

Remark 2: The primary objective of the event-triggered scheme is to strike an optimal balance between system dynamics and computational burden. To achieve this balance, it is imperative for designers to meticulously determine the parameters involved in the event-triggered condition (7), specifically ρ^p, Φ, and σ. In the initial phase, designers must assess the actuators' capabilities to ascertain the feasibility of executing control actions within the system. Within the operational bounds of the actuators, designers must then factor in the anticipated system performance. Notably, within the matrix Φ, higher values should be assigned to elements corresponding to states of greater interest. Regarding $\rho^p (p = 1, 2, \cdots, \bar{p})$, its value should decrease as the order of p increases. This is attributed to the fact that the most recently released signal exerts the most significant influence on system dynamics. The selection of σ is intimately tied to the desired frequency of the event-triggered scheme. Opting for a lower frequency necessitates choosing a smaller value for σ, and vice versa.

It is worth noting that the improved ETS offers two supplementary advantages. Firstly, in contrast to the traditional event-triggered conditions that solely relied on the differences between the current measurement and the most recently released one, the improved ETS incorporates multiple historic triggered signals to construct the event-triggered condition, which is beneficial to trigger some important signals at the crest or trough of the state response curves. Secondly, compared to the traditional ETSs [33], the improved ETS is less prone to triggering less significant points due to larger load disturbances.

III. Robust Cooperative LFC for Multi-area Power Systems

A. Improved LFC Model

This work adopts the thermal plant as the base power. The system dynamics consists of five parts, with the subscript $i = 1, 2, \cdots, M$ indexing the i-th area. These five parts are generator, governor, power system, tie-line power, and area control error [24], whose dynamics are respectively represented by

$$\Delta \dot{P}_{m_i} = -\frac{1}{T_{d_i}} \Delta P_{m_i} + \frac{1}{T_{d_i}} \Delta P_{v_i}, \tag{8}$$

$$\Delta \dot{P}_{v_i} = -\frac{1}{R_i T_{g_i}} \Delta f_i - \frac{1}{T_{g_i}} \Delta P_{v_i} + \frac{1}{T_{g_i}} \Delta P_{c_i}, \tag{9}$$

$$\begin{aligned} \Delta \dot{f}_i = &-\frac{D_i}{T_{m_i}} \Delta f_i + \frac{1}{T_{m_i}} \Delta P_{m_i} - \frac{1}{T_{m_i}} \Delta P_{\text{tie}}^i \\ &+ \frac{1}{T_{m_i}} \Delta P_{W_i} - \frac{1}{T_{m_i}} \Delta P_{L_i}, \end{aligned} \tag{10}$$

$$\Delta \dot{P}_{\text{tie}}^i = \sum_{j=1, j\ne i}^{M} 2\pi T_{ij} (\Delta f_i - \Delta f_j), \tag{11}$$

$$ACE_i = \vartheta_i \Delta f_i + \Delta P_{\text{tie}}^i, \tag{12}$$

where the physical significance of system parameters are given in Table II.

TABLE II
PARAMETER METRICS

Parameters	Physical significance
Δf_i	deviation of frequency
ΔP_{W_i}	the wind power deviation
ΔP_{m_i}	deviation of generator mechanical power
ΔP_{v_i}	deviation of turbine value position
ΔP^i_{tie}	net tie-line active power flow
ΔP_{L_i}	load disturbance
T_{d_i}	time constant of generator
T_{g_i}	time constant of governor
T_{m_i}	time constant of power system
R_i	speed drop
D_i	equivalent damping coefficient of generator
T_{ij}	tie-line synchronizing coefficient between area i and j
ϑ_i	frequency bias constant $\vartheta_i = 1/R_i + D_i$

A more general LFC model for area i considering parameter variation due to the shift of operating point can be represented by

$$\begin{cases} \dot{x}_i = (\mathcal{A}_i + \Delta\mathcal{A}_i(t))x_i + \sum\limits_{j=1,j\neq i}^{M} \mathcal{A}_{ij}x_j + \mathcal{B}_i u_i + \mathcal{F}_i\omega_i, \\ y_i = \mathcal{C}_i x_i, \end{cases} \tag{13}$$

where x_i represents the state vector; u_i represents the control input; y_i signifies the measured output; ω_i denotes the load disturbance; $\Delta\mathcal{A}_i(t)$ is added to describe the potential variation of system parameters;

$$x_i = \begin{bmatrix} \Delta f_i & \Delta P_{m_i} & \Delta P_{v_i} & \Delta P^i_{\text{tie}} & \int ACE_i \end{bmatrix}^T,$$

$$\mathcal{A}_i = \begin{bmatrix} \frac{-D_i}{T_{m_i}} & \frac{1}{T_{m_i}} & 0 & \frac{-1}{T_{m_i}} & 0 \\ 0 & \frac{-1}{T_{d_i}} & \frac{1}{T_{d_i}} & 0 & 0 \\ \frac{-1}{R_i T_{g_i}} & 0 & \frac{-1}{T_{g_i}} & 0 & 0 \\ \sum\limits_{j=1,j\neq i}^{N} 2\pi T_{ij} & 0 & 0 & 0 & 0 \\ \vartheta_i & 0 & 0 & 1 & 0 \end{bmatrix},$$

$$\mathcal{A}_{ij} = \begin{bmatrix} 0 & 0 & 0 & 0 & 0 \\ 0 & 0 & 0 & 0 & 0 \\ 0 & 0 & 0 & 0 & 0 \\ -2\pi T_{ij} & 0 & 0 & 0 & 0 \\ 0 & 0 & 0 & 0 & 0 \end{bmatrix}, \ \mathcal{C}_i^T = \begin{bmatrix} \vartheta_i & 0 \\ 0 & 0 \\ 0 & 0 \\ 1 & 0 \\ 0 & 1 \end{bmatrix},$$

$$\mathcal{B}_i = \begin{bmatrix} 0 & 0 & \frac{1}{T_{g_i}} & 0 & 0 \end{bmatrix}^T,$$

$$\mathcal{F}_i = \begin{bmatrix} \frac{-1}{T_{m_i}} & 0 & 0 & 0 & 0 \\ \frac{1}{T_{m_i}} & 0 & 0 & 0 & 0 \end{bmatrix}^T,$$

$$\omega_i = \begin{bmatrix} \Delta P_{W_i} & \Delta P_{L_i} \end{bmatrix}^T.$$

Remark 3: The dynamics presented in Equations (8)-(12) are representative of small-signal LFC models. These models are characterized by parameter accuracy under conditions of minor load disturbances. However, when there is a substantial imbalance between power generation and consumption, often caused by those induced by high penetration of wind energy, the accuracy of linearized LFC models is compromised due to the shift of the steady-state operating point. To address the limitations of traditional LFC models [24], [28]–[32], the work of [33] has accounted for uncertainties in the speed droop coefficient within the governor dynamic, analyzing their implications on frequency regulation performance. It is noteworthy, however, that all parameters may undergo variations owing to the shift of the steady-state operating point, extending beyond the singular consideration of the speed droop coefficient. To account for the inherent variability of parameters in the small-signal model and to expand the applicability of the LFC model within the realm of electrical engineering, this paper introduces a more comprehensive characterization of parameter uncertainties denoted as $\Delta\mathcal{A}_i(t)$.

Since state measuring and feedback control of modern power systems are both realized by digital devices, e.g., phasor measurement units and remote telemetry units, the discrete-time state-space model is derived to streamline the subsequent discussions. The discrete-time representation of (13) is

$$\begin{cases} x_i(k+1) = (A_i + \Delta A_i(k))x_i(k) + B_i u_i(k) \\ \qquad\qquad + \sum\limits_{j=1,j\neq i}^{N} A_{ij}x_j(k) + F_i\omega_i(k), \\ y_i(k) = C_i x_i(k), \end{cases} \tag{14}$$

where $A_i = e^{\mathcal{A}_i h}$, $B_i = \int_0^h e^{\mathcal{A}_i s}\mathcal{B}_i ds$, $A_{ij} = e^{\mathcal{A}_{ij} h}$, $F_i = \int_0^h e^{\mathcal{A}_i s}\mathcal{F}_i ds$, and $C_i = \mathcal{C}_i$; h represents the sampling time; $\Delta A_i(k) = X_i G_i(k) Y_i$ is an uncertain matrix that is added to the traditional small-signal model, in which way we endeavor to explain the underlying shift of the operating point of power systems caused by the intermittent wind power output; X_i and Y_i denote two known matrices; $G_i(k)$ signifies an unknown but Lebesgue measurable matrix satisfying $G_i^T(k)G_i(k) \leq I$.

B. Cooperative Load Frequency Controller Design

The cooperative output feedback controller is designed as

$$u_i(k) = K_i y_i(k) + \sum_{j=1,j\neq i}^{M} K_{ij} y_j(k), \tag{15}$$

where K_i signifies the local controller gain; K_{ij} indicate the cooperative controller gains of the neighboring areas.

Based on (15), the closed-loop LFC model is formulated as

$$\begin{aligned} x_i(k+1) =& (A_i + \Delta A_i(k) + B_i K_i C_i)x_i(k) + F_i\omega_i(k) \\ &+ \sum_{j=1,j\neq i}^{N} (A_{ij} + B_i K_{ij} C_j)x_j(k). \end{aligned} \tag{16}$$

Next, we propose two theorems to realize robust cooperative LFC. Theorem 1 concerns the robust stability analysis, which ensures that there exist the feasible cooperative control gains.

Theorem 2 concerns the control synthesis, which facilitates the cooperative control gains selection.

C. Robust Stability Analysis

Before analyzing the robust stability for system (16), we firstly provide the definitions of asymptotic stability and robust stability.

Definition 1: The closed-loop cooperative LFC system (16) is asymptotically stable if

$$\lim_{k\to\infty} \|x_i(k)\|_2 = 0, \quad \forall\, \omega_i(k) = 0, \tag{17}$$

where $\|\cdot\|_2$ means the two-norm operator of a matrix.

Definition 2: The closed-loop cooperative LFC system (16) is asymptotically stable with Δf_i signal satisfying the predefined $\mathscr{H}_\infty$ performance index γ_i, if it is asymptotically stable, and under zero initial condition,

$$\|\Delta f_i\|_2^2 < \gamma_i^2 \|\omega_i\|_2^2, \quad \forall\, 0 \neq \omega_i \in l_2[0,\infty), \tag{18}$$

where $\|\Delta f_i\|_2^2 = \sum_{k=0}^{\infty} \Delta f_i^T(k)\Delta f_i(k)$, and $\|\omega_i\|_2^2 = \sum_{k=0}^{\infty} \omega_i^T(k)\omega_i(k)$.

Remark 4: To realize the stability of system frequency, the $\mathscr{H}_\infty$ performance index γ_i, which is a versatile metric that can be applied to any type of signal based on the designer's preference, is employed. Definition 2 outlines a robust $\mathscr{H}_\infty$ performance index that focuses on asymptotic stability. Specifically, the frequency deviation signal is chosen as the interested signal. Our aim is to limit the impact of wind power perturbations and load disturbances on the load frequency signals through the $\mathscr{H}_\infty$ performance index γ_i. The following Theorem 1 demonstrates the robust stability of multi-area power systems by performing the proposed method.

Theorem 1: The closed-loop cooperative LFC system (16) is asymptotically stable with the frequency deviation signal Δf_i satisfying the prescribed $\mathscr{H}_\infty$ performance index γ_i if there exist matrices $P_i > 0$, such that for $i = 1, 2, \cdots, M$,

$$\begin{bmatrix} \bar{A}^T P \bar{A} + D^T D - P & \bar{A}^T P F \\ * & F^T P F - \gamma^2 I \end{bmatrix} < 0, \tag{19}$$

where $*$ denotes the symmetric term of a sophisticated matrix, and

$$\begin{aligned}
\bar{A} &= A + BKC + \Delta A(k),\\
B &= \text{diag}\{B_1, B_2, \cdots, B_M\},\\
C &= \text{diag}\{C_1, C_2, \cdots, C_M\},\\
D &= \text{diag}\{D_1, D_2, \cdots, D_M\},\\
D_i &= [1,0,0,0,0], \quad i = 1, 2, \cdots, M,\\
F &= \text{diag}\{F_1, F_2, \cdots, F_M\},\\
P &= \text{diag}\{P_1, P_2, \cdots, P_M\},\\
\gamma &= \text{diag}\{\gamma_1, \gamma_2, \cdots, \gamma_M\},
\end{aligned}$$

$$A = \begin{bmatrix} A_1 & A_{12} & \cdots & A_{1M} \\ A_{21} & A_2 & \cdots & A_{2M} \\ \vdots & \vdots & \ddots & \vdots \\ A_{M1} & A_{M2} & \cdots & A_M \end{bmatrix},$$

$$K = \begin{bmatrix} K_1 & K_{12} & \cdots & K_{1M} \\ K_{21} & K_2 & \cdots & K_{2M} \\ \vdots & \vdots & \ddots & \vdots \\ K_{M1} & K_{M2} & \cdots & K_M \end{bmatrix}.$$

Proof: We design an area-dependent Lyapunov function for system (16) as

$$V(k) = \sum_{i=1}^{M} x_i^T(k) P_i x_i(k), \tag{20}$$

where P_i represents the Lyapunov matrix.

Further, by defining $x(k) = [x_1^T(k)\ x_2^T(k)\ \cdots\ x_M^T(k)]^T$, $\omega(k) = [\omega_1^T(k)\ \ \omega_2^T(k)\ \ \cdots\ \ \omega_M^T(k)]^T$, $\zeta(k) = \left[x^T(k)\, \omega^T(k)\right]^T$, one can derive

$$\begin{aligned}
\Delta V(k) &= V(k+1) - V(k)\\
&= \sum_{i=1}^{M} x_i^T(k+1) P_i x_i(k+1) - \sum_{i=1}^{M} x_i^T(k) P_i x_i(k)\\
&= \zeta^T(k) \begin{bmatrix} \bar{A}^T P \bar{A} - P & \bar{A}^T P F \\ * & F^T P F \end{bmatrix} \zeta(k)
\end{aligned}$$

When $\omega(k) = 0$, one can calculate

$$\Delta V(k) = x^T(k)(\bar{A}^T P \bar{A} - P)x(k). \tag{21}$$

Based on Theorem 1, $\Delta V(k) < 0$ is evidently established for any $x(k) \neq 0$, which ensures that system (16) is asymptotically stable.

For some disturbances in (16), we design the following performance index

$$\Xi(k) = \Delta V(k) + \Delta f^T(k)\Delta f(k) - \gamma^2 \omega^T(k)\omega(k), \tag{22}$$

where $\Delta f(k) = [\Delta f_1^T(k)\ \Delta f_2^T(k)\ \cdots\ \Delta f_M^T(k)]^T$.

Performing a summation over both sides of (22) with respect to $k = 0, 1, \cdots, \infty$, one derives

$$\begin{aligned}
\bar{\Xi} &= \sum_{k=0}^{\infty} \Xi(k)\\
&= V(\infty) - V(0) + \sum_{k=0}^{\infty} \Delta f^T(k)\Delta f(k)\\
&\quad -\gamma^2 \sum_{k=0}^{\infty} \omega^T(k)\omega(k).
\end{aligned} \tag{23}$$

From Theorem 1, $\bar{\Xi} < 0$ is obviously established. From $V(\infty) \geq 0$ together with $V(0) = 0$, $\|\Delta f\|_2^2 < \gamma^2 \|\omega\|_2^2$ is established for $\omega \in l_2[0,\infty)$. Thus, Theorem 1 holds. ■

D. Robust Controller Gains Selection

Attentive readers may notice that the sufficient condition derived in Theorem 1, i.e., (19), can hardly be handled by standard linear matrix inequality (LMI) toolbox in Matlab due to the matrix coupling between the robust cooperative

controller gain K and the Lyapunov matrix P. Furthermore, the sufficient condition (19) accounts for the variation of system parameters represented by $\Delta A(k)$, which is a time-varying and unknown matrix. To address these two challenges, we introduce Theorem 2 that employs the inequality transformation and the cone complementarity linearization (CCL) approach to facilitate the robust controller gains selection.

Theorem 2: The closed-loop cooperative LFC system (16) is asymptotically stable with the frequency deviation signal Δf_i satisfying the prescribed $\mathscr{H}_\infty$ performance index γ_i if there exist matrices $P_i > 0$, $O_i > 0$, and a scalar $\kappa > 0$, such that for $i = 1, 2, \cdots, M$,

$$\begin{bmatrix} -O & A+BKC & F & X \\ * & D^TD - P + \kappa Y^TY & 0 & 0 \\ * & * & -\gamma^2 I & 0 \\ * & * & * & -\kappa I \end{bmatrix} < 0, \quad (24)$$

$$PO = I, \quad (25)$$

where

$$X = \text{diag}\{X_1, X_2, \cdots, X_M\},$$
$$Y = \text{diag}\{Y_1, Y_2, \cdots, Y_M\},$$
$$O = \text{diag}\{O_1, O_2, \cdots, O_M\}.$$

Proof: Using Schur complement to (24), one arrives at

$$\begin{bmatrix} -O & A+BKC & F \\ * & D^TD - P & 0 \\ * & * & -\gamma^2 I \end{bmatrix} + \kappa^{-1} \begin{bmatrix} X \\ 0 \\ 0 \end{bmatrix} \times \begin{bmatrix} X \\ 0 \\ 0 \end{bmatrix}^T + \kappa \begin{bmatrix} 0 \\ Y^T \\ 0 \end{bmatrix} \begin{bmatrix} 0 \\ Y^T \\ 0 \end{bmatrix}^T < 0. \quad (26)$$

Applying Young's inequality to (26), we can obtain

$$\begin{bmatrix} -O & A+BKC & F \\ * & D^TD - P & 0 \\ * & * & -\gamma^2 I \end{bmatrix} + \begin{bmatrix} X \\ 0 \\ 0 \end{bmatrix} \times G(k) \begin{bmatrix} 0 \\ Y^T \\ 0 \end{bmatrix}^T + \begin{bmatrix} 0 \\ Y^T \\ 0 \end{bmatrix} G^T(k) \begin{bmatrix} X \\ 0 \\ 0 \end{bmatrix}^T < 0, \quad (27)$$

that is

$$\begin{bmatrix} -O & \bar{A} & F \\ * & D^TD - P & 0 \\ * & * & -\gamma^2 I \end{bmatrix} < 0. \quad (28)$$

Applying Schur complement to (28) , one can obtain

$$\begin{bmatrix} D^TD - P & 0 \\ * & -\gamma^2 I \end{bmatrix} + \begin{bmatrix} \bar{A}^T \\ F^T \end{bmatrix} O^{-1} \begin{bmatrix} \bar{A}^T \\ F^T \end{bmatrix}^T < 0, \quad (29)$$

which is equivalent to

$$\begin{bmatrix} \bar{A}^T O^{-1} \bar{A} + D^TD - P & \bar{A}^T O^{-1} F \\ * & F^T O^{-1} F - \gamma^2 I \end{bmatrix} < 0. \quad (30)$$

Defining $O_i = P_i^{-1}$, one can arrive at (19). By employing CCL, one can obtain the robust cooperative gains automatically through LMI toolbox in Matlab. Hence, Theorem 2 is proved. ■

IV. Validations

A. System Parameters and Robust Cooperative LFC

The simulation employs a four-area fully connected power system (see Fig. 2), and each area is integrated with 100 wind turbines. The base power capacity of the power system is $400MW$. The rated power of each wind turbine is $2MW$, corresponding to $i_{qr}^{\text{ref}} = 1.75A$ and $\Omega_s = 1.17rad/s$. The parameters of wind turbine of each area are introduced in Table III [37]. The parameters involved in event-triggered MPC are $Q = \text{diag}\{1, 1\}$, $N = 5$, $S = 1$, $\rho^1 = 0.6$, $\rho^2 = 0.3$, $\rho^3 = 0.1$, $\sigma = 0.2$, $\Phi = \text{diag}\{1, 1\}$. The parameters of the four-area power system are given in Table IV [32]. The parameters involved in DLFC are $h = 1s$, $M = [0.01; 0.01; 0.01; 0.01; 0.01]$, $N = M^T$, $G(k) = 0.1\text{sin}(10k)$, $\gamma = 0.5$, $T_m(k) = 0.03(\text{rand} - 0.5)$, $\Delta P_{L_i} = 0.01(\text{rand} - 0.5)$, rand $\in [0, 1]$ denotes a uniform-distributed random number.

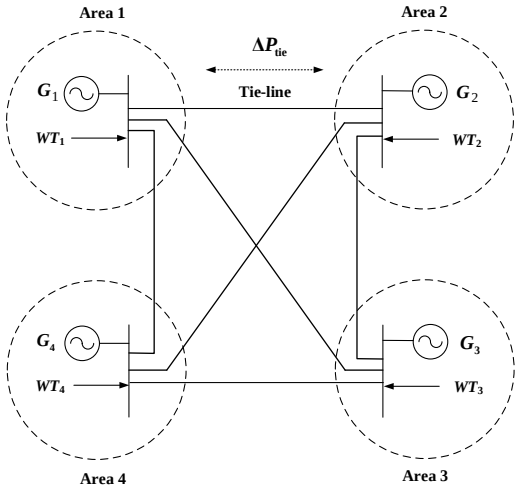

Fig. 2. Structure of the four-area power system with wind turbines.

TABLE III
PARAMETERS OF THE WIND TURBINE

Ω_s	R_r	R_s	L_s	L_m	L_r	M_t
1.17	0.00552	0.00491	0.09273	3.9654	0.1	4.5

TABLE IV
PARAMETERS OF THE POWER SYSTEM WITH $T_{ij} = 0.1$

Area 1	Area 2	Area 3	Area 4
$D_1 = 5$	$D_2 = 1$	$D_3 = 3$	$D_4 = 4$
$T_{m_1} = 20$	$T_{m_2} = 14$	$T_{m_3} = 11$	$T_{m_4} = 9$
$T_{d_1} = 1.2$	$T_{d_2} = 1.0$	$T_{d_3} = 0.7$	$T_{d_4} = 0.5$
$T_{g_1} = 1.2$	$T_{g_2} = 0.6$	$T_{g_3} = 1.4$	$T_{g_4} = 0.8$
$R_1 = 0.016$	$R_2 = 0.03$	$R_3 = 0.05$	$R_4 = 0.08$

B. Validations of Rated Wind Power Tracking and Improved ETS

This section examines the rated wind power tracking control through the analysis of two-state dynamics of each individual wind turbine, namely the rotor current and rotational speed, as depicted in Fig. 3. i_{qr} and Ω fluctuate at the reference values, $1.75A$ and $1.17rad/s$, respectively. This is attributable to the mechanical torque disturbance. Specifically, i_{qr} displays a fluctuation with an amplitude of $0.005A$, whereas Ω exhibits a more pronounced fluctuation with an amplitude of $0.01rad/s$. Moreover, the dynamics of the rated wind power output P_w is simulated for a cluster of 100 wind turbines, as illustrated in Fig. 4. The resulting total power fluctuation, arising from the aggregation of 100 wind turbines, is observed to have an amplitude of $2MW$, which is equivalent to 1% of the total capacity of $200MW$ and is deemed acceptable for renewable energy supply to the main grid. This result verifies the efficacy of the MPC in realizing rated wind power tracking.

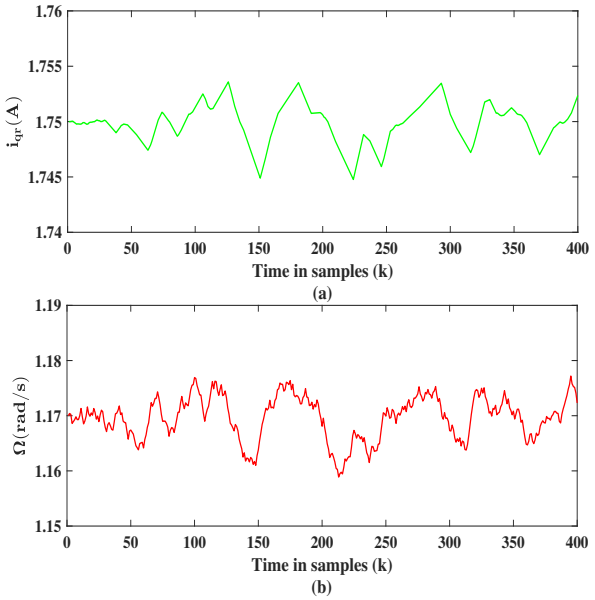

Fig. 3. Dynamics of states of the wind turbine. (a) Dynamic of i_{qr}. (b) Dynamic of Ω.

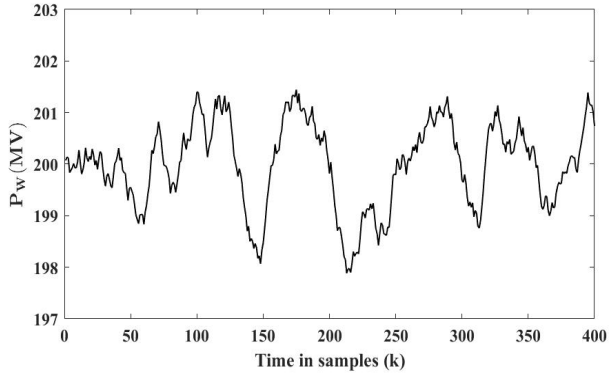

Fig. 4. Power dynamic P_w of 100 wind turbines.

Fig. 5 demonstrates the control actions for rated wind power tracking under the improved ETS. It presents a compelling evidence that the improved ETS is capable to relieve the computational burden of the MPC. Specifically, Fig. 5(a) depicts the control actions at each time instant, with each horizontal line segment indicating the corresponding idle time of the controller. This visualization reveals that the improved ETS enables the controller to be in an idle state for extended periods without compromising the control performance. Furthermore, Fig. 5(b) provides a graphical representation of the event-triggered instants and intervals, which clearly illustrates that the controller does not need to seek an optimal control action for a significant portion of the time, with the maximal idle time of 17 seconds. Both Fig. 5(a) and Fig. 5(b) provide a strong empirical support for the efficacy of the presented ETS in relieving the computational burden of the MPC without sacrificing the control performance.

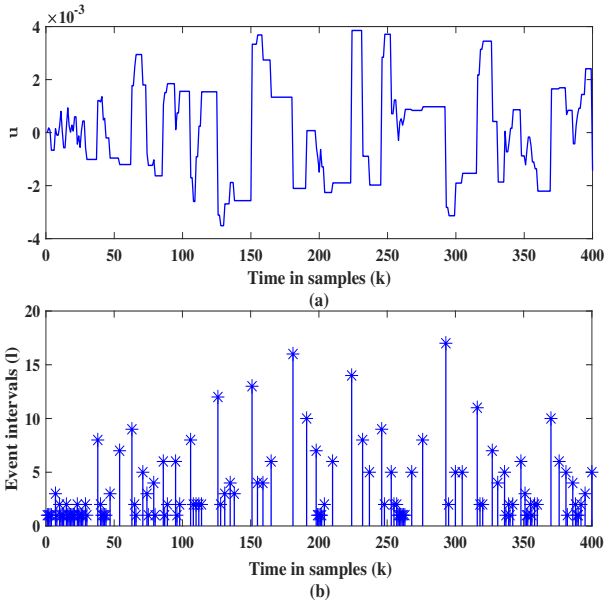

Fig. 5. Control actions and improved ETS. (a) Control actions. (b) Event-triggered times and intervals.

C. Validations of Robust Cooperative LFC With Wind Turbines

To test the superiority of the proposed robust cooperative LFC strategy, the following three control methods are considered for comparison.

1) *Controller 1:* Typical PI controller with control gains $K_1 = [0.3, -0.06]$, $K_2 = [0.6, -0.03]$, $K_3 = [1.2, -0.05]$, $K_4 = [0.9, -0.04]$, and $K_{ij} = [0, 0]$ for $i, j = 1, \cdots, 4, i \neq j$ [33].
2) *Controller 2:* The robust cooperative controller based on the traditional small-signal LFC model [24], whose control gains are given in Table V.
3) *Controller 3:* The proposed robust cooperative controller based on the improved small-signal LFC model, whose control gains are automatically selected through Theorem 2 and are shown in Table VI.

TABLE V
ROBUST COOPERATIVE CONTROLLER GAINS BASED ON THE TRADITIONAL SMALL-SIGNAL LFC MODEL

Area	Local controller gain	Cooperative controller gains
Area 1	$K_1 = [0.4617, -0.1519]$	$K_{12} = [0.0293, -0.0040]$ $K_{13} = [0.0471, -0.0043]$ $K_{14} = [0.0569, -0.0046]$
Area 2	$K_2 = [0.4194, -0.0746]$	$K_{21} = [0.0071, -0.0016]$ $K_{23} = [0.0187, -0.0017]$ $K_{24} = [0.0114, -0.0001]$
Area 3	$K_3 = [1.3312, -0.1585]$	$K_{31} = [0.0111, -0.0025]$ $K_{32} = [0.0171, -0.0024]$ $K_{34} = [0.0325, -0.0027]$
Area 4	$K_4 = [1.9816, -0.1078]$	$K_{41} = [0.0060, -0.0014]$ $K_{42} = [0.0078, -0.0012]$ $K_{43} = [0.0156, -0.0015]$

TABLE VI
ROBUST COOPERATIVE CONTROLLER GAINS BASED ON THE IMPROVED SMALL-SIGNAL LFC MODEL

Area	Local controller gain	Cooperative controller gains
Area 1	$K_1 = [0.5013, -0.1124]$	$K_{12} = [-4.4788e-3, 4.3022e-4]$ $K_{13} = [-1.8421e-5, -7.2387e-5]$ $K_{14} = [-7.1164e-3, 6.0357e-4]$
Area 2	$K_2 = [0.4954, -0.0681]$	$K_{21} = [-1.6710e-3, 2.3808e-4]$ $K_{23} = [-5.3971e-3, 5.7360e-4]$ $K_{24} = [1.2171e-3, -1.0808e-4]$
Area 3	$K_3 = [1.7418, -0.1498]$	$K_{31} = [-5.3517e-3, 6.8330e-4]$ $K_{32} = [-1.4061e-2, 1.9566e-3]$ $K_{34} = [-2.9988e-2, 2.6449e-3]$
Area 4	$K_4 = [1.3521, -0.1089]$	$K_{41} = [-1.0409e-3, 4.0752e-5]$ $K_{42} = [5.4974e-4, -6.3710e-5]$ $K_{43} = [-4.7161e-3, 5.0851e-4]$

Fig. 6 illustrates the frequency deviation dynamics of four areas with the penetration of wind energies under the initial conditions $\Delta f_1(0) = 0.1Hz$, $\Delta f_2(0) = 0.08Hz$, $\Delta f_3(0) = 0.06Hz$, $\Delta f_4(0) = 0.04Hz$, in which red lines illustrate the dynamics under *Controller 1*, green lines indicate the dynamics under *Controller 2*, and blue lines demonstrate the dynamics under *Controller 3*. Evidently, with the traditional PI controller, the largest amplitude of the frequency deviation among four areas is about $0.3Hz$. Due to the fact that the admissible frequency deviation is $\pm 0.2Hz$ of LFC, the traditional PI controller is incapable to regulate the frequency with such a high penetration level ($200MW$) of wind energy. In contrast to the traditional PI controller, the robust cooperative controller based on the traditional small-signal LFC model can maintain the frequency deviation within the limit of $\pm 0.2Hz$, which means that *Controller 2* is feasible in regulating the frequency with $200MW$ wind energy integration. By further comparing the frequency dynamics between *Controller 2* and *Controller 3*, we can see that with the improved small-signal LFC model (considering the potential shift of the steady-state operating point and model this property by adding an uncertain but bounded matrix in traditional small-signal model), the proposed robust cooperative controller is capable of regulating the frequency to the much smaller overshoot. This verifies that the proposed robust cooperative LFC approach is effective to smooth the high penetration of wind energy and outperforms the other two controllers.

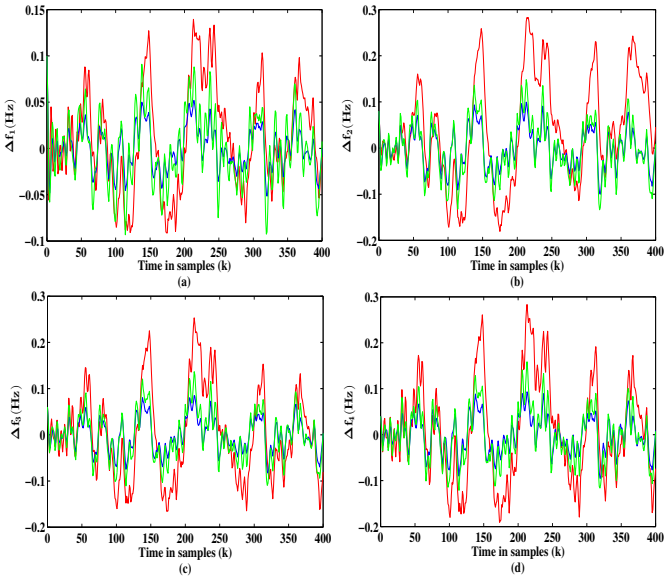

Fig. 6. Frequency deviation dynamics of four areas with the penetration of wind energies. Red lines indicate the dynamics under *Controller 1*. Green lines indicate the dynamics under *Controller 2*. Blue lines indicate the dynamics under *Controller 3*.

D. Validations of Robust Cooperative LFC Considering Communication Delays

For a practical power system, various underlying adversarial factors can lead to communication delays among areas during the transmission of system states. These factors include network congestion, bandwidth limitations, environmental elements such as interference, signal attenuation, and obstacles, as well as hardware or software failures in the communication infrastructure. As a consequence, based on the results in Section IV.C, we further verify the efficacy of the presented robust cooperative LFC approach considering communication delays. In the case study, the communication delays can occur between any different communication links within the networked structure (see Fig. 2) and are modeled by stochastic function with the upper bound set as 3 times of the sampling period h.

In an illustrative representation of communication delays, Fig. 7 depicts a specific scenario characterized by stochastic delays in the communication link between area 3 and area 2. Accordingly, Fig. 8 portrays the frequency deviation dynamics, taking into account the influence of communication delays. It becomes evident from Fig. 8 that the proposed robust cooperative LFC approach, which considers the potential shift of the steady-state operating point (referred to as *Controller 3*), consistently outperforms the alternative controllers (referred to as *Controller 1* and *Controller 2*), even though there are communication delays within the networked control structure.

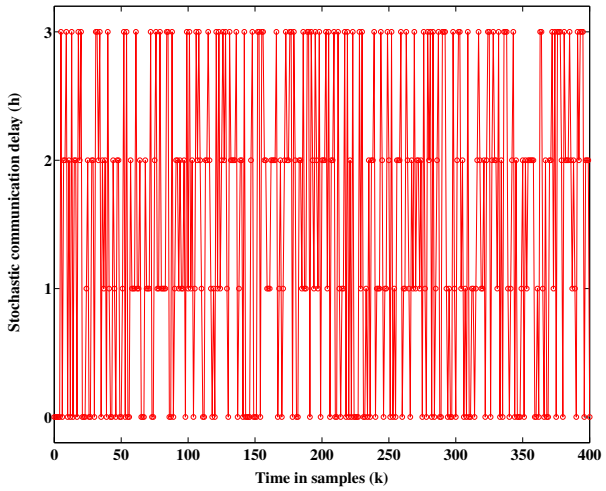

Fig. 7. Demonstration of communication delays from area 3 to area 2.

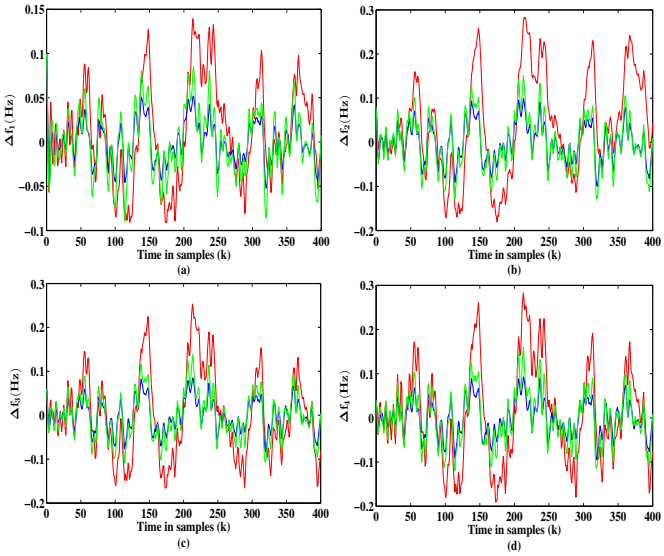

Fig. 8. Frequency deviation dynamics of four areas considering stochastic communication delays. Red lines indicate the dynamics under *Controller 1*. Green lines indicate the dynamics under *Controller 2*. Blue lines indicate the dynamics under *Controller 3*.

V. Conclusion

The paper concerns the robust cooperative LFC for multi-area power systems with the participation of wind turbines. To smoothly accommodate the wind power, a hierarchical control structure is presented. The MPC is used to track the rated wind power in low-level wind turbine control, in which an improved ETS considering a series of historic released signals is developed to reduce the computational burden. In high-level cooperative LFC, robust performance is incorporated in the frequency controller design to smooth the integration of wind energy to the main grid. Besides, to extend the applicability of the LFC model with the penetration of wind energy, the work adds an uncertain matrix to explain the potential shift of the operating point caused by the intermittent wind power supply. Simulations are conducted on a four-area power system with each area penetrated with $200MW$ wind energy. The results validate that the improved ETS is efficient in reducing the computational burden of MPC, and that the proposed robust cooperative LFC approach is more applicable in maintaining the frequency deviation within the limit of $\pm 0.2Hz$, compared to the traditional PI controller and the small-signal model based controller.

References

[1] D. K. Panda, S. Das, and S. Townley, "Toward a more renewable energy-based LFC under random packet transmissions and delays with stochastic generation and demand," *IEEE Transactions on Automation Science and Engineering*, vol. 19, no. 2, pp. 1217–1232, 2022.

[2] Y. Li, H. Zhang, X. Liang, and B. Huang, "Event-triggered-based distributed cooperative energy management for multienergy systems," *IEEE Transactions on Industrial Informatics*, vol. 15, no. 4, pp. 2008–2022, 2019.

[3] L. Chen, J. Mei, C. Li, and G. Ma, "Distributed leader–follower affine formation maneuver control for high-order multiagent systems," *IEEE Transactions on Automatic Control*, vol. 65, no. 11, pp. 4941–4948, 2020.

[4] Y. Li, B. Huang, J. Dai, D. W. Gao, Q. Sun, and H. Zhang, "Distributed resilient initialization-free Jacobi descent algorithm for constrained optimization against DoS attacks," *IEEE Transactions on Automation Science and Engineering*, DOI:10.1109/TASE.2023.3278865.

[5] R. Ma, Z. Hu, H. Yang, Y. Jiang, M. Huo, H. Luo, and R. Yang, "Adversarial FDI attack monitoring: Toward secure defense of industrial electronics," *IEEE Industrial Electronics Magazine*, DOI:10.1109/MIE.2023.3292988.

[6] Z. Hu, R. Su, K.-V. Ling, Y. Guo, and R. Ma, "Resilient event-triggered MPC for load frequency regulation with wind turbines under false data injection attacks," *IEEE Transactions on Automation Science and Engineering*, DOI: 10.1109/TASE.2023.3337006.

[7] B. Fan and X. Wang, "Distributed privacy-preserving active power sharing and frequency regulation in microgrids," *IEEE Transactions on Smart Grid*, vol. 12, no. 4, pp. 3665–3668, 2021.

[8] Q. Wei, G. Shi, R. Song, and Y. Liu, "Adaptive dynamic programming-based optimal control scheme for energy storage systems with solar renewable energy," *IEEE Transactions on Industrial Electronics*, vol. 64, no. 7, pp. 5468–5478, 2017.

[9] F. Liu, C. Chen, C. Lin, G. Li, H. Xie, and Z. Bie, "Utilizing aggregated distributed renewable energy sources with control coordination for resilient distribution system restoration," *IEEE Transactions on Sustainable Energy*, vol. 14, no. 2, pp. 1043–1056, 2023.

[10] V. Veerasamy, L. P. M. I. Sampath, S. Singh, H. D. Nguyen, and H. B. Gooi, "Blockchain-based decentralized frequency control of microgrids using federated learning fractional-order recurrent neural network," *IEEE Transactions on Smart Grid*, vol. 15, no. 1, pp. 1089–1102, 2024.

[11] H. H. Alhelou, H. Parthasarathy, N. Nagpal, V. Agarwal, H. Nagpal, and P. Siano, "Decentralized stochastic disturbance observer-based optimal frequency control method for interconnected power systems with high renewable shares," *IEEE Transactions on Industrial Informatics*, vol. 18, no. 5, pp. 3180–3192, 2022.

[12] H. Zhao, Q. Wu, S. Huang, M. Shahidehpour, Q. Guo, and H. Sun, "Fatigue load sensitivity-based optimal active power dispatch for wind farms," *IEEE Transactions on Sustainable Energy*, vol. 8, no. 3, pp. 1247–1259, 2017.

[13] M. Shojaee and S. M. Azizi, "Decentralized robust control of a coupled wind turbine and diesel engine generator system," *IEEE Transactions on Power Systems*, vol. 38, no. 1, pp. 807–817, 2023.

[14] K. Zhang, R. Su, and H. Zhang, "A novel resilient control scheme for a class of Markovian jump systems with partially unknown information," *IEEE Transactions on Cybernetics*, vol. 52, no. 8, pp. 8191–8200, 2022.

[15] Z. Hu, S. Liu, W. Luo, and L. Wu, "Intrusion-detector-dependent distributed economic model predictive control for load frequency regulation with PEVs under cyber attacks," *IEEE Transactions on Circuits and Systems I: Regular Papers*, vol. 68, no. 9, pp. 3857–3868, 2021.

[16] Y. Zhang, X. Liu, and B. Qu, "Distributed model predictive load frequency control of multi-area power system with DFIGs," *IEEE/CAA Journal of Automatica Sinica*, vol. 4, no. 1, pp. 125–135, 2017.

[17] L. Dai, T. Zhou, Z. Qiang, Z. Sun, and Y. Xia, "Distributed economic mpc for dynamically coupled linear systems: A Lyapunov-based approach," *IEEE Transactions on Systems, Man, and Cybernetics: Systems*, vol. 53, no. 3, pp. 1408–1419, 2023.

[18] M. Vali, V. Petrović, L. Y. Pao, and M. Kühn, "Model predictive active power control for optimal structural load equalization in waked wind farms," *IEEE Transactions on Control Systems Technology*, vol. 30, no. 1, pp. 30–44, 2022.

[19] Z. Hu, R. Su, K. Zhang, Z. Xu, and R. Ma, "Resilient event-triggered model predictive control for adaptive cruise control under sensor attacks," *IEEE/CAA Journal of Automatica Sinica*, vol. 10, no. 3, pp. 807–809, 2023.

[20] Q. Wei, D. Liu, F. L. Lewis, Y. Liu, and J. Zhang, "Mixed iterative adaptive dynamic programming for optimal battery energy control in smart residential microgrids," *IEEE Transactions on Industrial Electronics*, vol. 64, no. 5, pp. 4110–4120, 2017.

[21] H. Zhang, C. Qin, and Y. Luo, "Neural-network-based constrained optimal control scheme for discrete-time switched nonlinear system using dual heuristic programming," *IEEE Transactions on Automation Science and Engineering*, vol. 11, no. 3, pp. 839–849, 2014.

[22] G. Liu, Q. Sun, R. Wang, and X. Hu, "Nonzero-sum game-based voltage recovery consensus optimal control for nonlinear microgrids system," *IEEE Transactions on Neural Networks and Learning Systems*, vol. 34, no. 11, pp. 8617–8629, 2023.

[23] K. Zhang, R. Su, H. Zhang, and Y. Tian, "Adaptive resilient event-triggered control design of autonomous vehicles with an iterative single critic learning framework," *IEEE Transactions on Neural Networks and Learning Systems*, vol. 32, no. 12, pp. 5502–5511, 2021.

[24] J. Hu, J. Cao, J. M. Guerrero, T. Yong, and J. Yu, "Improving frequency stability based on distributed control of multiple load aggregators," *IEEE Transactions on Smart Grid*, vol. 8, no. 4, pp. 1553–1567, 2017.

[25] X. Liang, C. Andalib-Bin-Karim, W. Li, M. Mitolo, and M. N. S. K. Shabbir, "Adaptive virtual impedance-based reactive power sharing in virtual synchronous generator controlled microgrids," *IEEE Transactions on Industry Applications*, vol. 57, no. 1, pp. 46–60, 2021.

[26] S. Liu, P. X. Liu, and X. Wang, "Stochastic small-signal stability analysis of grid-connected photovoltaic systems," *IEEE Transactions on Industrial Electronics*, vol. 63, no. 2, pp. 1027–1038, 2016.

[27] B. Fan and X. Wang, "Fault recovery analysis of grid-forming inverters with priority-based current limiters," *IEEE Transactions on Power Systems*, vol. 38, no. 6, pp. 5102–5112, 2023.

[28] A. Ghafouri, J. Milimonfared, and G. B. Gharehpetian, "Coordinated control of distributed energy resources and conventional power plants for frequency control of power systems," *IEEE Transactions on Smart Grid*, vol. 6, no. 1, pp. 104–114, 2015.

[29] S. Saxena and Y. V. Hote, "Load frequency control in power systems via internal model control scheme and model-order reduction," *IEEE Transactions on Power Systems*, vol. 28, no. 3, pp. 2749–2757, 2013.

[30] S. Doolla and T. Bhatti, "Load frequency control of an isolated small-hydro power plant with reduced dump load," *IEEE Transactions on Power Systems*, vol. 21, no. 4, pp. 1912–1919, 2006.

[31] C. Peng, J. Li, and M. Fei, "Resilient event-triggering H_∞ load frequency control for multi-area power systems with energy-limited DoS attacks," *IEEE Transactions on Power Systems*, vol. 32, no. 5, pp. 4110–4118, 2017.

[32] Z. Hu, S. Liu, W. Luo, and L. Wu, "Resilient distributed fuzzy load frequency regulation for power systems under cross-layer random denial-of-service attacks," *IEEE Transactions on Cybernetics*, vol. 52, no. 4, pp. 2396–2406, 2022.

[33] S. Liu, W. Luo, and L. Wu, "Co-design of distributed model-based control and event-triggering scheme for load frequency regulation in smart grids," *IEEE Transactions on Systems, Man, and Cybernetics: Systems*, vol. 50, no. 9, pp. 3311–3319, 2020.

[34] G. Liu, Q. Sun, R. Wang, and H. Zhang, "Event-based fuzzy adaptive consensus FTC for microgrids with nonlinear item via prescribed fixed-time performance," *IEEE Transactions on Circuits and Systems I: Regular Papers*, vol. 69, no. 7, pp. 2982–2993, 2022.

[35] K. Zhang, B. Zhou, W. X. Zheng, and G.-R. Duan, "Event-triggered and self-triggered gain scheduled control of linear systems with input constraints," *IEEE Transactions on Systems, Man, and Cybernetics: Systems*, vol. 52, no. 10, pp. 6452–6463, 2022.

[36] T. Yu, Y. Zhao, J. Wang, and J. Liu, "Event-triggered sliding mode control for switched genetic regulatory networks with persistent dwell time," *Nonlinear Analysis: Hybrid Systems*, vol. 44, p. 101135, 2022.

[37] J. B. Ekanayake, N. Jenkins, and G. Strbac, "Frequency response from wind turbines," *Wind Engineering*, vol. 32, no. 6, pp. 573–586, 2008.

Zhijian Hu (Member, IEEE) received the PhD degree in Control Science and Engineering from Harbin Institute of Technology, Harbin, China, in 2022. From 2019 to 2020, he was a Joint PhD Student with the Department of Electronics, Carleton University, Ottawa, Canada. He is currently a Research Fellow in the School of Electrical and Electronic Engineering, Nanyang Technological University, Singapore. His research interests include model predictive control, fault detection, resilient control, and the applications in power systems and microgrids. He served as the Associate Editor of Journal of Intelligent and Fuzzy Systems, and the Session Chair of IFAC WC 2023. He was the recipient of the Marie Skłodowska-Curie Postdoctoral Fellowship in 2023.

Kun Zhang (S'18-M'20) received the Ph.D. degree in control theory and control engineering from the Northeastern University, China. He was a research fellow with School of Electrical and Electronic Engineering, NTU, and a special research assistant with the Institute of Systems Science, AMSS, CAS, before he joined Beihang University. Currently, he is an associate professor in the School of Astronautics. His main research interests include system optimization, learning control, and their industrial applications. Dr. Zhang was the Session Chair or PC Member in IEEE-ICCA, CCC, CSIS-IAC, etc. He was awarded the 2022 Wu Wenjun AI Science & Technology Award (Recipient of Outstanding PhD Nomination), and was a recipient of Best Prize in the China Automation Congress (CAC 2019) IET CSR Outstanding Paper.

Rong Su (Senior Member, IEEE) obtained his Bachelor of Engineering degree from University of Science and Technology of China, and Master of Applied Science degree and PhD degree from University of Toronto, respectively. He was affiliated with University of Waterloo and Technical University of Eindhoven before he joined Nanyang Technological University in 2010. Dr Su's research interests include multi-agent systems, discrete-event system theory, model-based fault diagnosis, cyber security analysis and synthesis, control and optimization of complex networks with applications in flexible manufacturing, intelligent transportation, human-robot interface, power management and green building. In the aforementioned areas he has more than 300 journal and conference publications, 2 monograph, 18 granted/filed patents. Dr Su is a senior member of IEEE, and an associate editor for IEEE Transactions on Cybernetics, Automatica (IFAC), Journal of Discrete Event Dynamic Systems: Theory and Applications, and Journal of Control and Decision. He was the Chair of the Technical Committee on Smart Cities in the IEEE Control Systems Society in 2016-2019. Currently, he is a co-chair of Technical Committee on Automation in Logistics in the IEEE Robotics and Automation Society. Dr Su is the recipient of 2021 Hsue-shen Tsien Paper Award from IEEE/CAA Journal of Automatica Sinica, a Distinguished Lecturer for 2020 Chinese Conference on Decision and Control (CCDC'20) and an IEEE Distinguished Lecturer for IEEE Robotics and Automation Society.

Ruiping Wang received the Bachelor degree in Electrical Engineering from China University of Mining and Technology, Xuzhou, China, in 2015, the Master degree in Control Engineering from Harbin Engineering University, Harbin, China, in 2017. He is currently pursuing the PhD degree in Control Science and Engineering from Beihang University, Beijing, China. His research interests include intelligent control, deep learning, and the applications in autonomous driving.

Yushuai Li (M'19) received the B. S. degree in electrical engineering and automation, and the Ph.D. degree in control theory and control engineering from the Northeastern University, Shenyang, China, in 2014 and 2019, respectively. He is currently a Marie Curie Researcher at the Department of Informatics, University of Oslo, Norway. He received the Best Paper Awards from Journal of Modern Power Systems and Clean Energy and 2023 International Conference on Cyber-energy Systems and Intelligent Energies (ICCSIE). His main research interests include distributed optimization and control, machine learning, digital twin, and their applications in integrated energy and transportation systems.